Design and Evaluation of a Bidirectional Soft Glove for Hand Rehabilitation-Assistance Tasks

Jianwei Lai, Aiguo Song, *Senior Member, IEEE*, Ke Shi, Qinjie Ji, *Graduate Student Member, IEEE*, Ye Lu, and Huijun Li

***Abstract*—Soft pneumatic gloves are a promising tool for assisting stroke patients with hand dysfunction in their rehabilitation and daily activities. However, current gloves have limited extension force output. This article presents a hybrid actuator that combines a silicone flexion actuator with an extension actuator made from shape memory alloy (SMA) springs. The Critical parameters and material of the soft actuator were optimized using a finite element model. Additionally, the SMA spring actuator was equipped with a water-cooling structure to reduce temperature and increase response speed by 55.8%. The hybrid actuator generated an obstructed tip force of 16.02 N at 200 kPa pressure and an extension force of 8.675 N. The hybrid actuator was integrated with the water-cooling structure into a soft glove and evaluated in trials involving eight stroke patients. With the assistance of the glove, the bending angles of the stroke patients' index fingers, including the PIP and MCP joints, significantly improved, increasing from 6.8 ± 2.8° and 11.3 ± 4.6° to 68.3 ± 5.3° and 68.1 ± 5.5°, respectively. Furthermore, the glove also increased the maximum friction with a 50-mm cylinder from 8.4 ± 3.5 N to 21.34 ± 5.8 N.**

***Index Terms*—Hybrid actuator, rehabilitation robotics, wearable robotics, soft robot materials and design.**

I. Introduction

STROKE and sports injuries may result in the loss of motor functions in the hand. Such motor dysfunction hinders the independent life of stroke patients and reduces the patient's quality of life [1]. Repetitive task practices are helpful in the rehabilitation of stroke patients. As the demand for clinicians increases, it is increasingly difficult to meet the rehabilitation needs of patients [2]. The rapid development of robotics can help with this problem [3], as robots can efficiently and accurately complete tasks assigned by a therapist. The motion trajectory of rigid exoskeleton rehabilitation robots can be preset through a linkage structure [4]. However, the rotation center of the robot is difficult to align with the patient's joints during the movement. This reduces the wearability and comfort of the rehabilitation device.

Soft rehabilitation gloves have attracted extensive research attention due to the characteristics of the soft material [5], which improves safety and comfort in the rehabilitation process. Correia et al. proposed a soft actuator [6] that enables the output of multiple degrees of freedom from a single input and realizes movement in the rehabilitation gloves by restricting the motion of the soft actuator in the nonfunctional direction. Cappello et al. developed a fiber rope-constrained soft actuator to assist finger flexion [7], while Yang et al. optimized the airbag parameters to obtain a soft actuator with a larger bending angle and higher driving efficiency [8]. These gloves based on soft actuators assist the flexion motion of the patient. However, during rehabilitation, patients also require extension motion [9], [10], [11]. Some patients have high muscle tone [12], [13], but despite this residual force in the hands, they cannot fully extend their fingers.

Several teams have developed soft actuators to assist finger extension and flexion movements. Passive devices pull the fingers to an extended state using a spring [10], but this physical element modifies the transparency of the finger, thus affecting its normal bending behavior. Chen et al. proposed a dual-channel actuator that realizes bidirectional bending movements [14]. However, the thickness of the airbag presents an obstacle to large bending angles, which prevents the actuator from realizing sufficient bending of the fingers. Yap et al. developed a fabric-based soft actuator that can be driven in two directions, with movement generated by pressurizing the airbag [11]. Unfortunately, as the angle of the fabric-based soft actuator decreases, the output force will also decrease. Kazeminasab et al. developed a soft glove based on a shape memory alloy (SMA) spring actuator [15], with the temperature switching crystal state of the SMA spring actuator used to control the grip force of the glove [16]. The volume of this driving method is small, but the output force is too small to assist finger flexion. Kang et al. proposed a cable-driven glove that assists the patient's fingers in two directions [17]. This driving method introduces parasitic forces during the rehabilitation process [18], and cannot provide sufficient force to assist the fingers. In summary, developing a soft rehabilitation glove that generates enough output force and bending angle

Manuscript received 1 September 2022; revised 5 March 2023 and 25 May 2023; accepted 20 June 2023. Date of publication 7 July 2023; date of current version 9 August 2023. This article was recommended for publication by Associate Editor E. Mastinu and Editor P. Dario upon evaluation of the reviewers' comments. This work was supported in part by the Natural Science Foundation of China under Grant 92148205 and Grant 62173088, and in part by the Frontier Leading Project of Jiangsu Basic Research Program under Grant BK20192004. *(Corresponding author: Aiguo Song.)*

This work involved human subjects or animals in its research. Approval of all ethical and experimental procedures and protocols was granted by the Ethics Committee of Zhongda Hospital, Southeast University under Application No. 2020ZDSYLL088-P01.

The authors are with the State Key Laboratory of Bioelectronics, Jiangsu Key Lab of Remote Measurement and Control, School of Instrument Science and Engineering, Southeast University, Nanjing 210096, China (e-mail: a.g.song@seu.edu.cn).

Digital Object Identifier 10.1109/TMRB.2023.3292414

Fig. 1. Prototype of the bidirectional soft rehabilitation glove.

TABLE I
COMPARISON OF ACTUATOR CAPACITY

	Bending Angle	Extension Force	Flexion Force	Drive Method
Polygerinos *et al.* [19]	250°	0 N	7.3 N	Soft Actuator
Yap *et al.* [11]	182°	3.1 N*	14.3 N	TPU Actuator
Kang *et al.* [17]	165°	7 N	7 N	Cable Drive
Saharan *et al.* [20]	73°	2.84 N	2.84 N	SMA Drive
Required Value	161° [21]	6 N* [22]	12 N [23]	-
This work	191.3°	8.675 N	16.02 N	Hybrid Actuator

*Note: the output force of the thermoplastic polyurethane (TPU) actuator is 0.31 Nm [11], and the muscle tension of the metacarpophalangeal (MCP) joint is 0.6 Nm [22]. Nm is a moment unit, not a force unit. For a better comparison, the length of the adult index finger is about 0.1 m. In this case, 0.31 Nm and 0.6 Nm are approximately equal to 3.1 N and 6 N, respectively.

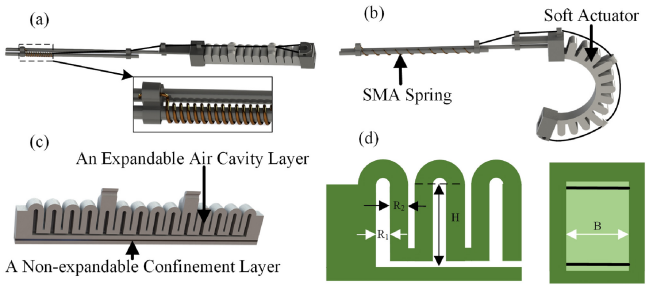

Fig. 2. (a) Extension state of the actuator. (b) Flexion state of the actuator. (c) Cross-sectional view of the soft actuator. (d) Key parameter information of soft actuator.

to assist the patient's finger flexion and extension movements is a challenging task.

This article describes a soft rehabilitation glove based on a hybrid actuator that combines a soft actuator and an SMA spring actuator (see Fig. 1). Table I compares several critical parameters of the proposed hybrid actuator with those of existing actuators, such as the bending angle, extension force, and flexion force. It shows that the hybrid actuator assists the patient's fingers to perform flexion and extension movements, and that the output force and working space satisfy the needs of rehabilitation and activities of daily living (ADLs). The design, optimization and performance evaluation of the proposed actuator were investigated. The actuator was integrated into the soft glove, and a control system was designed. Two control strategies were implemented for daily life assistance and rehabilitation training: a button mode and a mirror rehabilitation training. This study evaluated the performance of a soft robotic glove that users controlled through a mobile phone interface. A clinical trial was conducted to test the efficacy of the glove in improving grip strength and finger range of motion in individuals. Eight participants with unilateral paralysis were recruited and provided informed consent prior to participating in the trial. The main contributions of this study can be summarized as follows:

1) A hybrid actuator was designed, which combines a soft actuator and an SMA spring actuator. This hybrid actuator can generate enough output force and bending angle to assist patients in performing flexion and extension movements.
2) A water-cooling structure was developed and connected to the SMA spring actuator. This cooling structure reduces the reaction time by 55.8% compared to conventional actuators and has a time ratio of 2.3:1. It is also quieter and easier to fabricate.
3) By combining the hybrid actuator with the water-cooling structure, a soft and wearable rehabilitation glove was designed to assist patients in rehabilitation and ADLs.

In the following sections, we introduce the design, optimization and performance evaluation of the proposed actuator. The bidirectional soft glove is then studied, including the integration, the control algorithm, and the interactive graphical interface of the proposed device. Finally, trials have been conducted to validate the performance of the proposed device.

II. HYBRID ACTUATOR DESIGN, FABRICATION AND VERIFICATION

Soft actuators have been extensively studied. Polygerinos et al. proposed a soft glove based on segmented soft actuators [24], which can assist the flexion motion of the fingers. Yang et al. modeled a soft actuator and increased the actuator's bending angle and output force by optimizing its parameters [8], whereas Mosadegh et al. researched a soft actuator [25] in which a reduced gas mass enables an increased response speed. Dilibal et al. proposed a soft robotic gripper made of thermoplastic polyurethane (TPU) [26], and used finite element analysis (FEA) to optimize the critical parameters. Analysis of the needs of patients in clinical trials indicates that the soft actuators used for hand rehabilitation must satisfy several requirements: a) They should provide the fingers with a greater working space [21] (metacarpophalangeal (MCP): 40°, proximal interphalangeal (PIP): 64°, distal interphalangeal (DIP): 57°) and more significant output force [23] (output force: 12 N) to meet the needs of finger rehabilitation and ADLs. b) They should help the flexion and extension of the patient's fingers. c) Their material should be soft and comfortable to wear.

A. Design of the Hybrid Actuator

We have established a hybrid actuator composed of a soft actuator and an SMA spring actuator (see Fig. 2(a)). The soft actuator consists of an expandable air cavity layer and a non-expandable confinement layer (see Fig. 2(c)). The expandable layer contains gaps between each chamber's inner walls. It is designed such that the two contact surface walls are thinner than the other walls, and the contact surface area is more extensive. Therefore, the increased internal pressure preferentially expands the contact wall and minimizes the strain generated on the other walls. In addition, the proximity of the two adjacent chambers causes the raised inner walls to push against each other. This leads to a preferential elongation of the extensible layer, while its height increases by less than 0.5 mm at an air pressure of 150 kPa. In addition, the soft actuators can be quickly manufactured using 3D printed molds to iterate different designs.

The SMA is a nickel–titanium alloy that has previously been used as an intelligent actuator [27]. The crystal transformation of the material allows the SMA to recover from deformed shapes caused by external pressure or through temperature changes. The alloy's two phases of austenite and martensite can be transitioned by modifying the temperature [28]. The positive transformation is from the austenite phase to the martensite phase, starting at the martensite starting temperature (M_s) and ending at the martensite ending temperature (M_f). The reverse transformation is from the martensite phase to the austenite phase, starting from the austenite starting temperature (A_s) and ending at the austenite ending temperature (A_f).

Based on the above analysis, a hybrid actuator is developed that combines a soft actuator and an SMA spring actuator. In the finger flexion process (as shown in Fig. 2(b)), the soft actuator is pressurized to generate the bending motion and synchronously assist the finger in flexion movement. At the same time, the SMA spring actuator is in the martensite phase because the temperature is below A_s. In this case, the stiffness of the SMA spring actuator is small, and so it hardly affects the bending of the soft actuator. In the process of finger extension (as shown in Fig. 2(a)), the SMA spring actuator is heated by a current and transforms into the austenite state. At the same time, the soft actuator is deflated. The SMA spring actuator returns to the compressed state to assist the finger extension movement. In this way, the actuator can realize movement in both the flexion and extension directions.

B. Parameter Optimization of Soft Actuator

The critical parameters and materials of the soft actuator are optimized to increase the output force and working space of the actuator, as shown in Fig. 2(d). The parameters of interest include the width of the air cavity B, height of the air cavity H, intermediate radius R_1, radius of the air cavity R_2, and material of the soft actuator. To improve the bending angle and output force of the soft actuator, Yang et al. have researched the influence of the critical parameters on each aspect of performance [8].

The impact of each parameter on performance is now analyzed separately. The bending angle of the actuator increases as the air cavity width B increases. However, when the width is too large, the freedom of movement between the fingers is negatively affected. The width of the air cavity is set to $B = 16$ mm; this is the same width as the fingers. Increasing the air cavity height H enhances the bending angle of the actuator, but also increases the weight of the actuator. To reduce the load on the fingers, considering the bending angle and the weight of the glove, the height of the air cavity is set to $H = 15$ mm. The distance between the air cavities R_1 has a slight effect on the bending angle of the actuator. An increase in the number of cavities can improve the bending angle of the actuator, so the width between the air chambers is set to $R_1 = 1.2$ mm; this is the maximum precision allowed by our 3D printer.

The output force of the actuator increases as the radius of the air cavity R_2 increases, but the bending angle of the actuator simultaneously decreases. Similarly, an increase in the Shore hardness of the soft actuator material results in an increase in output force, but a decrease in the bending angle. However, increasing the bending angle of the actuator can improve the working space of the fingers. In addition, increasing the output force of the actuator allows the actuator to overcome the patient's muscle tension and produce a corresponding training effect. A sufficient bending angle and output force play a significant role in the rehabilitation of patients. It is difficult to obtain the ideal value of the cavity radius R_2 and material of the soft actuator.

We simulated and optimized the cavity radius R_2 and material of the soft actuator. To improve the actuator's performance, FEA was conducted using ANSYS. FEA is a valuable method for the analysis of soft actuators. Through FEA, the performance of actuators with different pneumatic pressures can be determined. In optimizing the air cavity, the radius R_2 was set to 2 mm, 3 mm, and 4 mm in turn, and the material was Dragon Skin 30 (Smooth-on Inc., PA, USA). In the optimization of the material, the thickness of the cavity was set to 3 mm, and actuators made of Ecoflex 50 (Smooth-on Inc.), Dragon Skin 10 (Smooth-on Inc.), and Dragon Skin 30 were analyzed.

As the clamping structure has little effect on the bending of the soft actuator, it was simplified in the simulations. In the FEA simulation process, the SMA spring actuator was neglected to reduce the impact of inaccurate modeling of this component. In the model, the strain limiting layer was made of paper and modeled with shell elements SHELL181 [8]. The paper has a linear elastic characterization with Young's modulus of E = 1.2 GPa, a Poisson's rate of $\mu = 0.2$, and a thickness of $\delta = 0.09$ mm. According to the literature [29], [30], the property of Dragon Skin 10 was built as a Yeoh model, the strain energy potential U is independent from the second invariant:

$$U = \sum_{i=1}^{N} C_{i0}\left(\bar{I}_1 - 3\right)^i, \tag{1}$$

where $\bar{I}_1$ is the first deviatoric strain invariant and C_{ij} is a material specific parameter. the material coefficients were $N = 3$, $C_{10} = 3.6 \times 10^4 J \cdot m^{-3}$, $C_{20} = 258 J \cdot m^{-3}$, and $C_{30} = -0.56 J \cdot m^{-3}$. Similarly, the property of Dragon Skin 0030 was built as a Yeoh model with parameter values $N = 2$,

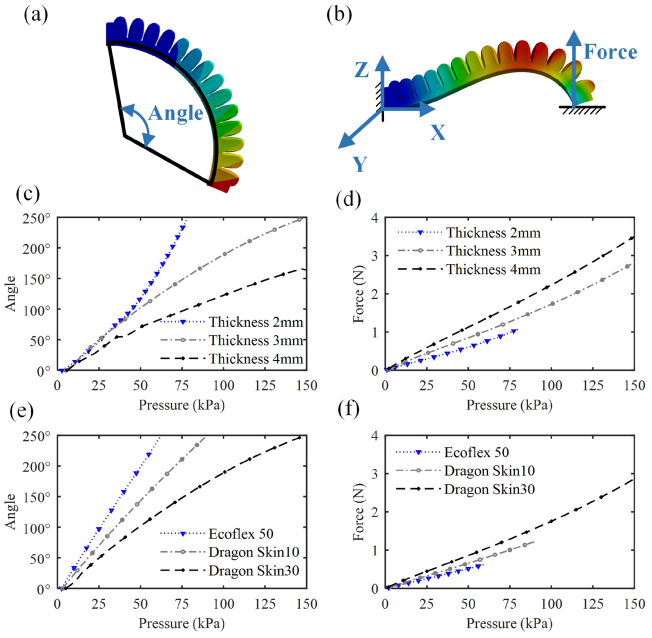

Fig. 3. (a) Simulation results of the bending angle of the actuator. (b) Simulation results of the output force at the end of the actuator. (c) Comparison of bending capacity of actuators with thicknesses of 2 mm, 3 mm, and 4 mm. (d) Simulation results of the output force of actuators with thicknesses of 2 mm, 3 mm, and 4 mm. (e) Comparison of the bending angle of actuators made of Ecoflex 50, Dragon Skin 10, and Dragon Skin 30. (f) Comparison of output forces of different actuators made of Ecoflex 50, Dragon Skin 10, and Dragon Skin 30.

$C_{10} = 1.19 \times 10^3 J \cdot m^{-3}$, and $C_{20} = 2.3028 \times 10^4 J \cdot m^{-3}$. The property of Ecoflex 0050 was built as an Ogden model, and the strain energy potential U is a function of deviatoric principal stretches λ_i. The following relation for incompressible materials represents it:

$$U = \sum_{i=1}^{N} \frac{2\mu_i}{\alpha_i^2}\left(\lambda_1^{\alpha_i} + \lambda_2^{\alpha_i} + \lambda_3^{\alpha_i} - 3\right), \tag{2}$$

where μ_i and α_i are empirical parameters. The material coefficients were $N = 3$, $\alpha_1 = 1.55$, $\mu_1 = 107.9 \times 10^3 J \cdot m^{-3}$, $\alpha_2 = 7.86$, $\mu_2 = 21.47 J \cdot m^{-3}$, $\alpha_3 = -1.19$, and $\mu_3 = -87.1 \times 10^3 J \cdot m^{-3}$. These components were glued together in order, and the constraints between each element were applied. The contact surfaces share the same node. In addition, the adjacent surfaces of each chamber unit interact under a certain pressure. Therefore, friction constraints were applied to adjacent surfaces. Considering the soft actuator's carrying capacity and the simulation's convergence, the pressure range of the simulation was set to 0–150 kPa. Pressure loading was applied to the actuator over this range at intervals of 5 kPa. At the same time, to ensure consistency between the output angle and the output force, the air pressure was set to stop increasing when the output angle of the actuator exceeded 250°.

The influence of the air cavity pressure on the bending angle of the actuator is shown in Fig. 3(a), which shows that the bending angle of the actuator is driven by the expansion of the air cavity unit. Except for the installation and positioning unit, each unit has the same deformation. The influence of the pressure of the air cavities on the output force is shown in Fig. 3(b). The opposite output force of the end plane is used as the output force of the actuator.

The influence of the radius of the air cavity R_2 on the bending angle of the soft actuator is shown in Fig. 3(c). The pressure of the air cavities is positively correlated with the bending angle of the actuator. For $R_2 = 4$ mm, the bending angle of the actuator reaches 165° at an air pressure of 150 kPa. And the output angle of the actuator can exceed 250° when the radius of the air cavity is 2 mm or 3 mm. The 3-mm air cavity radius gives the best linear relationship with the bending angle. The simulation results showing the end output force of the soft actuator for different values of R_2 are shown in Fig. 3(d). The output force of the actuator has a direct proportional relation with the air pressure. $R_2 = 4$ mm gives the largest output force of the actuator. However, the bending angle of the actuator at 150 kPa is less than 250°. The output force of the actuator with $R_2 = 2$ mm reaches 1.07 N when the air pressure is 80 kPa. For $R_2 = 3$ mm, the output force reaches 2.8 N when the air pressure is 150 kPa. So, the radius of the air cavity is set to $R_2 = 3$ mm.

The bending angle of actuators made of different materials with respect to the air pressure is shown in Fig. 3(e). The three actuator materials exhibit similar trends. These actuators can achieve a bending angle of 250° under different air pressures. The Shore hardness of the material affects the actuator's stiffness and bending angle. The distal side output force of the different actuator materials is shown in Fig. 3(f). The trends vary depending on the material. The actuator made of Ecoflex 50 generates an end output force of 0.62 N, while the actuators made of Dragon Skin 10 and Dragon Skin 30 output 1.22 N and 2.8 N, respectively. The bending angle of the actuator made of three materials can exceed 250°, satisfying the ADL's need. Additionally, the actuator made of Dragon Skin 30 can output the most significant output force. So the actuator material is selected Dragon Skin 30.

C. Water-Cooling Structure of the SMA Spring Actuator

The driving method of the SMA spring actuator is similar to that of human muscle. It has the characteristics of being quiet during driving and a high power-to-quality ratio. This characteristic can help the soft actuator increase the extension driving force without increasing the volume of the actuator too much. To obtain a more significant deformation displacement, the SMA is made to have a spring form. The end of the SMA spring actuator is connected to the soft actuator through a cable, while the guide rail formed by the round tube fully contacts the SMA spring actuator. The SMA spring actuator is cooled by water to increase its response speed. The diameter of the SMA spring actuator is 4.75 mm, the number of coil turns is 20, and the wire diameter of the SMA is 0.5 mm. The M_s, M_f, A_s, A_f of the SMA is 12° C, 24° C, 45° C, 64° C respectively. Some researches have suggested that the appropriate frequency of the rehabilitation is 5 times per minute [31]. SMA spring response times do not meet the speed requirements of rehabilitation training. In order to improve the response frequency of the hybrid actuator, we design the cooling structure for the SMA spring.

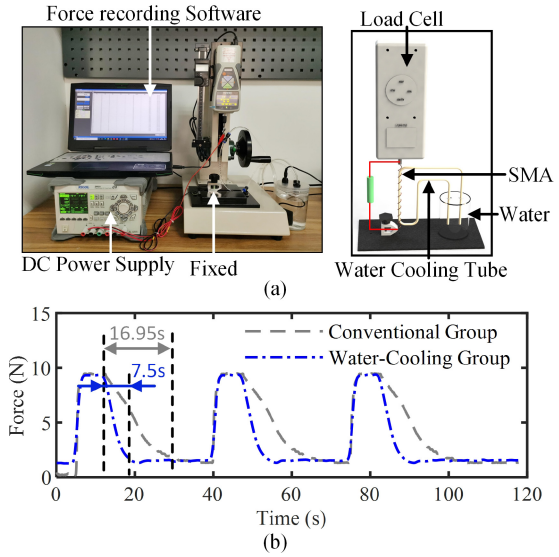

Fig. 4. (a) Experimental platform of SMA spring actuator. (b) Force output curves of conventional and water-cooled SMA spring actuators.

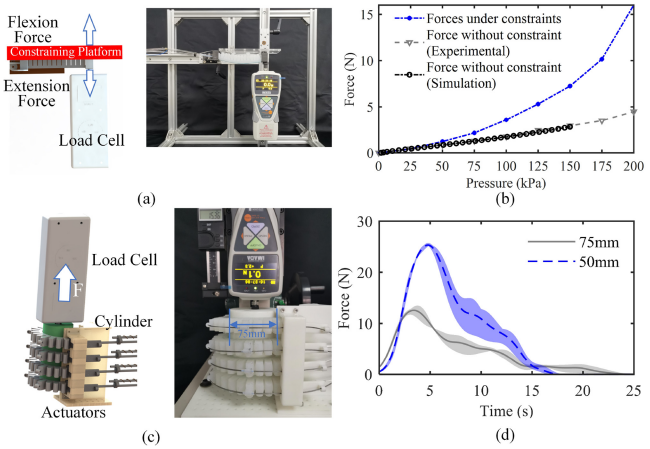

Fig. 5. (a) Schematic diagram of force measurement system for measuring the force of the blocking tip applied by an soft actuator or SMA spring actuator. (b) The force curve of the hybrid actuator in the extension direction. (c) Friction force exerted by the actuator on the load cell during the pressurization process. (d) Friction output curve of the actuator.

Experiments were carried out to characterize the SMA spring actuator's output force and verify the effect of the proposed cooling structure. The experimental platform is shown in Fig. 4(a). A programmable direct current (DC) power supply is connected to the SMA spring actuator to provide current. A load cell (ZTS-50 N; Imada Co., Ltd., Toyohashi, Japan) is installed on the force measurement platform. The load cell has an accuracy of 0.01 N and a force measurement range of 0-50 N. Recording software installed on the computer allows the output force to be recorded in real time. The SMA spring actuator is fixed to the experimental platform, and the water tube in the middle contacts the SMA spring actuator to provide rapid cooling. This experiment considers both conventional and water-cooled actuators. In each case, the SMA spring actuator is heated with a current of 3.5 A after 5 s and then the current is cut off after 15 s; the total control period is 35 s. In the experiments, the water-cooling structure of the SMA spring actuator is not included in the conventional actuator. The water-cooling tube is shown in Fig. 4(a). The water has an initial temperature of 25.3° C.

The experimental results are shown in Fig. 4(b). In the water-cooling group, the SMA spring actuator requires 7.5 ± 0.19 s to pass from martensite to austenite, during which time the force drops from 9.4 N ± 0.82 N to 1.4 ± 0.73 N. Similarly, the conventional SMA spring actuator requires 16.95 ± 0.27 s to change phase, during which time the force drops from 9.4 ± 1.56 N to 1.8 ± 0.73 N. There is no significant difference in the force produced by the water-cooled actuator. However, compared with the conventional actuator, the reaction time has been reduced by 55.8%. The proposed cooling structure has a time ratio of 2.3:1. It has a better cooling effect than increasing stress (1.2:1) and using solid heat sink materials (2:1) [9]. These results prove the effectiveness of the cooling structure.

The heating and cooling experiments were repeated for 30 min. There were no significant changes in the water temperature. This may be because the cooling part of the system has a sufficiently large contact area with the air. The temperature increase caused by the SMA spring actuator has no significant effect on the water temperature over a long operation time. Due to the residual force of the SMA spring actuator, it is difficult to reduce the output force to zero after cooling, which will affect the transparency of the actuator. As the residual energy is minimal, this does not have a significant effect on the use of the actuator.

D. Hybrid Actuator Characterization

This experiment was carried out to characterize the actuator in terms of the non-obstructed tip force, the obstructed tip force, and the friction force applied to the cylinder.

The non-obstructed tip force was measured by a force measurement platform, including a freely movable two-axis motion platform and a ZTS-50N (see Fig. 5(a)). The actuator is connected to a pressure gauge, air pump, and control system. The non-obstructed tip force of the actuator, as shown in Fig. 5(b), increases as the air pressure increases. Under a pressure of 150 kPa, the non-obstructed tip force of the actuator is 2.92 N. The actuator can achieve a greater output force by increasing the air pressure. When the air pressure is 200 kPa, the non-obstructed tip force of the actuator is 4.047 N. The maximum force error between the actual output force and the simulation result is 6.1%. This demonstrates the ability of the model to predict the force exertion at the tip of the actuator.

Regarding the force output capability of the hybrid actuator in the extension direction, three constant force commands were used: 1 N, 5 N, 10 N. These commands are in the range of force applied in actual rehabilitation. For each command, three trials have been performed. And for each trial, the mean value of the force obtained at a steady state was calculated. Then, the mean and standard variation for each trial was calculated for each command. As shown in Table II, the percentage of change is around 11.9%, proving the hybrid actuator can output a stable force in the extension direction.

TABLE II
THE FORCE OF THE ACTUATOR IN THE EXTENSION DIRECTION

Force Command	1 N	5 N	10 N
Mean	1.253 N	4.264 N	8.675 N
Standard Deviation	0.015 N	0.197 N	0.023 N
Percentage of Variation	11.9%	4.6%	2.6%

The end side of the actuator was mounted onto a measurement platform to measure the obstructed tip force. During the pressurization process, a restriction platform was installed on one side of the actuator. This restrains and reduces the change of curvature of the actuator. This force measurement method is similar to that used in previous research [11]. Limiting the surface of the actuator minimizes the effect of nonlinearities caused by changes in the actuator's curvature when pressurized. As shown in Fig. 5(b), the obstructed tip force of the actuator increases with increasing air pressure. The obstructed tip force reaches 16.02 N under a pressure of 200 kPa.

The friction force of the fingers generated by the actuator is important in allowing patients to grasp objects. It effectively offsets the weight of the objects to prevent them from falling. The ZTS-50N was used to test the friction force exerted by the actuator. The corresponding four-finger actuator was pressurized to 150 kPa to bend cylinders with diameters of 50 mm and 70 mm (see Fig. 5(c)). This actuator was fixed on the test platform through the 3D printed parts. The cylinder was moved upward at a fixed speed using the mobile platform until being released from the actuator. The friction force generated by the actuator was recorded using software on the computer. The experiment was repeated three times. The data and average results of the three experiments are shown in Fig. 5(d). The results show that the maximum friction forces generated by the actuators are 12.72 $\pm$ 0.89 N (75 mm) and 25.69 $\pm$ 0.26 N (50 mm). From the highest point, the friction force fluctuates significantly as the actuator begins to slide. The friction force has an inverse relationship with the diameter of the cylinder. The experimental results show that the output friction of the actuator can reach the 1.2 kg required for daily life [23]. However, the force transfer between the actuator and the finger reduces the force with which the actuator assists the finger grip. To further evaluate the output friction of the hybrid actuator, the experiment was carries out in Section IV.

III. INTEGRATION OF SOFT GLOVES

A. Actuator Integration

The soft rehabilitation glove consists of five soft actuators and a cotton glove (see Fig. 6(a)). The hybrid actuators and cotton gloves are connected by flexible Velcro. It increases the comfort and safety of patient fingers and reduces the effects of kinematics differences between actuators and fingers [32]. A Teflon tube is installed between the cable and the soft actuator to reduce the energy loss caused by friction [17]. Similarly, a Teflon tube is installed at the end of the hybrid actuator to reduce interference between different finger motions.

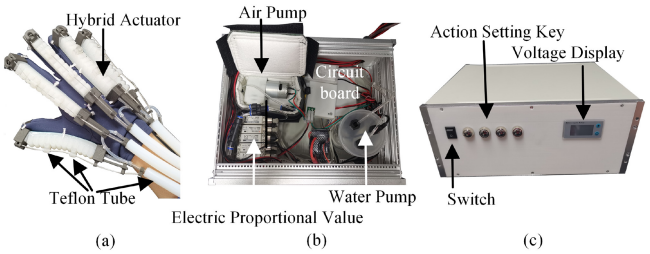

Fig. 6. Prototype of the bidirectional soft glove. (a) Back view of the glove. (b) Control system view. (c) Control box of the system, including switches, action selection buttons, and voltage display panel.

The control system is equipped with an air pressure control system and an SMA spring control system, and each actuator can be individually controlled (see Fig. 6(b)). The system consists of an air pump, water pump, force sensor, position sensor, electric proportional valve (ITV0030, SMC, Tokyo, Japan), lithium battery, and SMA spring actuator control circuit board. On each finger, a force sensor (FSR 402, Interlink Electronics, California, USA) is located on the fingertip to measure the force between the finger and the grasping object, and a flex sensor (FLEX2.2, Spectra Symbol, Utah, USA) is located on the back of the finger to measure the bending angle of the finger. To enhance the safety and reliability of the sensor, we have sewn the force and position sensors on the inside of the glove. To improve the patient's experience, we applied a layer of silica gel inside the glove to create adequate friction between the finger and the object. This ensured that the glove and fingers had the same friction coefficient. Additionally, we set a power switch on the control box, and the patient can turn off the power in an uncomfortable situation. The weight of the control system is 1312.5 g, and the weight of the glove is 317.7 g.

B. Controller Design

The Proportional Integral Derivative (PID) control algorithm is implemented on the microcontroller with a control frequency of 200 Hz. This algorithm is widely used for control loops in wearable robotic processes [11], [33], where physical models can be difficult to obtain. This is especially so in this study, where the flexure of the hybrid actuator is not easy to model. Therefore, the control scheme must be adaptable to accommodate a black box model. In addition, the parameters of the PID control algorithm are simple to adjust. For these reasons, the PID algorithm was selected for this work.

The force-position hybrid model combines position and force information into one control scheme [34], [35]. The main use cases for the proposed device include rehabilitation training and daily living assistance. In the rehabilitation training process, position control is employed to provide the patient with sufficient space for rehabilitation. During daily living assistance, force control is employed to assist the patient to grasp objects more safely and comfortably. In order to control both position and force, a force-position hybrid model was adopted as the control algorithm for this study. Due to the coupling relationship between force and position, the force-position hybrid model cannot control force and position

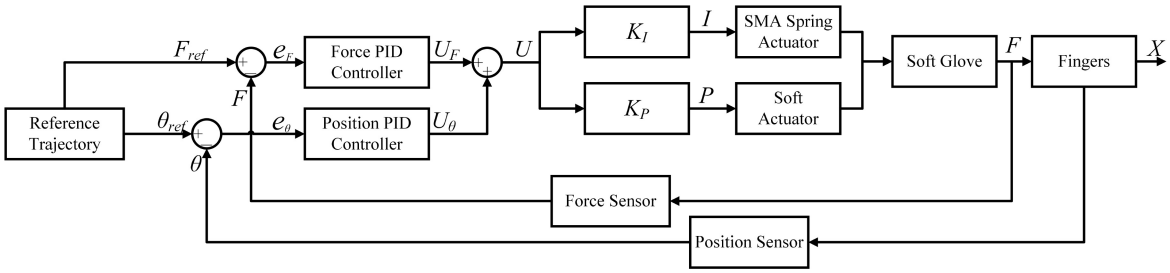

Fig. 7. Control implementation for each individual hybrid actuator.

accurately at the same time. In this system, we have tuned two control parameters corresponding to different operating modes, and they are biased towards position and force control, respectively.

Fig. 7 shows the control loop of this system. The PID algorithm is used as the control algorithm for force and position, which is defined as follows

$$U(k) = K_p e(k) + K_i \sum_{j=0}^{k} e(j) + K_d(e(k) - e(k-1)), \quad (3)$$

where e_θ represents the error between the designed finger's bending angle and the actual finger's bending angle, e_F represents the designed contact force and the actual contact force between the hybrid actuator and the finger, K_p, K_i, K_d are the proportional gain, the integral gain, and the derivative gain, respectively. The output value of the force controller and angle controller is $U = U_F + U_\theta$. According to the value U, the hybrid actuator selects the corresponding actuator. When the value $U > 0$, the air pressure of the soft actuator is set $P = UK_P$, where K_P is a parameter to be adjusted; and the current of the SMA spring actuator is set $I = 0$, thus the hybrid actuator assists the patient's finger flexion movement. When value $U < 0$, the current of the SMA spring actuator is set $I = UK_I$, where K_I is a parameter to be adjusted; and the air pressure of the soft actuator is set $P = 0$, thus the hybrid actuator assists the patient's finger extension movement.

C. Graphical Interactive Interface and Control Strategy

This system offers two control strategies: button mode and mirror rehabilitation training, both designed to assist chronic stroke patients with unilateral paralysis in their daily life and rehabilitation.

1) Control Strategy I–Button Mode: Hemiplegic patients may encounter difficulties with collaborative tasks that require the use of both hands, such as peeling fruit or brushing teeth. To address this challenge, a button mode was developed that enables patients to control a pair of gloves to produce specific hand gestures, allowing them to perform individual gestures necessary for daily life.

A graphical user interface (GUI), shown in Fig. 8, was created to operate the button mode through a mobile phone, enabling patients and clinicians to select the required gesture based on their needs. The unaffected finger of the patient is used to set the joint angle for the particular gesture in the joint angle setting. Several buttons in the control box,

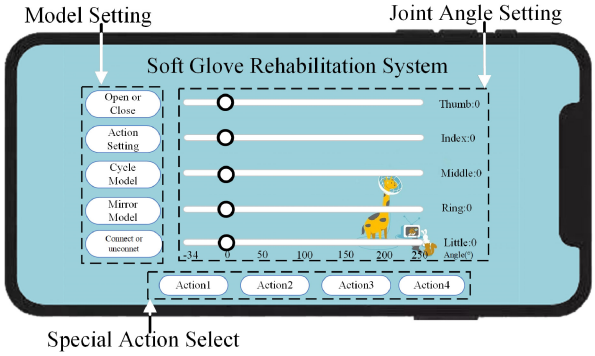

Fig. 8. Customized graphical user interface.

Fig. 9. Glove-assisted ADLs: (a) Pinching a pen. (b) Gripping a box. (c) Holding an apple.

shown in Fig. 6(c), achieve the same effect, making it convenient for patients to perform daily operations and rehabilitation training. The button mode can control the gloves to pinch a pen, grip a box, or hold an apple, as demonstrated in Fig. 9. These functions are advantageous for activities of daily living (ADLs).

2) Control Strategy II–Mirror Rehabilitation Training: This rehabilitation training system combines mirror therapy [36], robotic rehabilitation [37], and virtual reality [38] to aid chronic stroke patients with unilateral paralysis. The system, shown in Fig. 10, comprises soft gloves, a Leap motion sensor, and a computer with virtual scenes.

In the rehabilitation setup, the patient sits at a table with the affected hand wearing the glove. Using their unaffected hand, the patient interacts with a virtual scene. The Leapmotion sensor captures information about the joints in the patient's healthy hand fingers and transmits this data to the computer, which synchronizes the movements of the glove within the virtual scene. To control the soft glove, each finger is supported by a single hybrid actuator with a single degree of freedom underdrive control. The combined angles of the MCP and PIP joints, as measured by the flex sensor, serve as the

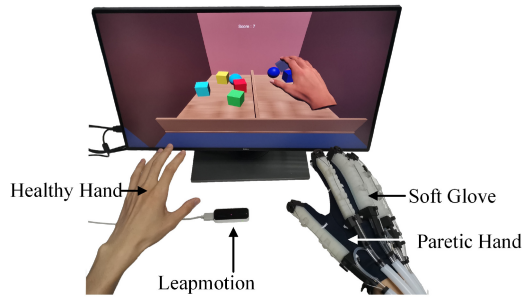

Fig. 10. Schematic diagram of hand rehabilitation training system based on mirror therapy.

actual angle value. Meanwhile, the combined angles of the MCP and PIP joints, as detected by Leapmotion, serve as the target value. Bilateral finger synchronization is accomplished through a force-position hybrid control algorithm implemented in the hybrid actuator. Simultaneously, the virtual scene displays the motion of the virtual finger, and the corresponding motion of the affected finger within the virtual scene stimulates the patient to generate motion in their affected finger.

This training strategy detects the voluntary movement of the patients, enabling them to control the overall process during rehabilitation. Studies have shown that mirrored training has a positive effect on hand rehabilitation [21]. The movement of the unaffected fingers is also maintained to prevent muscle atrophy on the healthy side. Additionally, we have designed rehabilitation tasks with different rehabilitation training games to cater to the various needs of patients. The system also allows a therapist to remotely customize the patient's rehabilitation tasks according to the patient's rehabilitation condition. Patients can complete the corresponding rehabilitation treatment without the presence of a therapist.

IV. Evaluation of Soft Gloves

The following experiments have been carried out to assess the rehabilitation robot's performance, including range of motion and grip strength.

A. Participants

The preliminary clinic was carried out in Zhongda Hospital Affiliated to Southeast University (Batch number: 2020ZDSYLL088-P01). Researchers and clinicians jointly formulated the research protocol, and suitable patients were included in the trial.

A total of 8 patients (5 males, 3 females, age 51.7 ± 11.0 years, onset time 18.6 ± 3.8 days;) participated in this trial. The inclusion criteria for the trial were stroke patients: (i) after 2 weeks and up to 1 year following stroke diagnosis; (ii) aged 25-75 years; (iii) could understand motor commands from therapist. Patients were excluded if they had: (i) psychiatric disorder or expressive apraxia; (ii) severe cognitive disorder (Mini-Mental State Examination <23); (iii) severe spasticity in any joints of the affected side (Modified Ashworth Scale >3). Eight patients matching the described criteria were enrolled in this study. The patient profiles are shown in Table III, and all patients completed the trial without interference.

TABLE III
Participant Characteristics

Subject	Gender	Age	Time Post-stroke	ARAT(66)	MAS(4)
S1	F	37	15 days	7	0
S2	M	57	16 days	6	1+
S3	M	68	18 days	11	2
S4	M	37	24 days	7	1
S5	M	59	16 days	3	0
S6	F	46	18 days	26	0
S7	M	52	17 days	14	2
S8	F	58	25 days	9	1

*Note: ARAT: The Action Research Arm Test. MAS: The Modified Ashworth Scale.

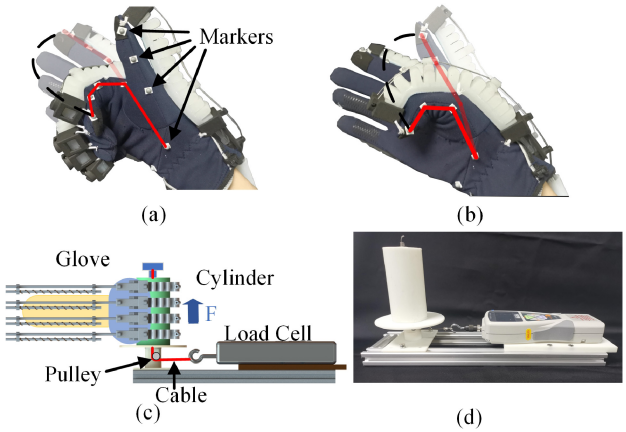

Fig. 11. (a) Reflective markers attached to the index finger to track the motion range during the bending of the index finger. (b) Reflective markers attached to the thumb to track the motion range during the bending of the thumb. (c) Schematic of portable device with a load cell for measuring glove-assisted grip strength. (d) Actual portable device with a load cell for measuring glove-assisted grip strength.

B. Data Recordings

A 3D optical motion capture system (Optitrack, NaturalPoint Inc., Corvallis, Oregon, USA) was used to evaluate the maximum range of the glove-assisted finger motion. The movement curves of the index finger and thumb were tracked. As shown in Fig. 11(a-b), four reflection markers were placed on the PIP, DIP, and MCP joints of the index finger. Four reflection markers were placed on the interphalangeal (IP), carpometa-carpal (CMC), and MCP joints of the thumb.

To measure the grip force provided by the gloves, a portable force-measuring device with a load cell was designed (as shown in Fig. 11(c-d)). Two cylindrical objects (50 mm and 75 mm radius, respectively) were used as grasping objects during the experiment.

C. Procedures

All participants provided written informed consent indicating their agreement to take part in the trial. They were seated in front of an adjustable-height table that allowed their hands to rest comfortably. The therapist placed a mobile phone

TABLE IV
MEAN (SD) CHANGES IN OUTCOMES MEASURES

Joint	Un-Assistive (UA)	ADL Required	Flexion Assistive (FA)	P-value (UA-FA)	Bidirection Assistive (BA)	P-value (UA-BA)	P-value (FA-BA)
Index DIP	11.9 ± 3.9°	57°	34.6 ± 4.3°	**	57.9 ± 7.9°	**	**
Index PIP	6.8 ± 2.8°	64°	41.1 ± 3.9°	**	68.3 ± 5.3°	**	**
Index MCP	11.3 ± 4.6°	40°	48.1 ± 3.5°	**	68.1 ± 5.5°	**	*
Thumb IP	9.6 ± 4.2°	18°	38.2 ± 5.3°	**	64.0 ± 4.4°	**	**
Thumb MCP	13.3 ± 3.5°	21°	14.8 ± 3.5°	P=0.51	32.6 ± 3.2°	**	**
CMC	8.5 ± 2.8°	5°	21.0 ± 4.4°	**	38 ± 3.9°	**	**

*Note: Data are presented as the mean ± SD.
Significant pairs respect to the baseline are presented with different levels: * $p < 0.05$, ** $p < 0.01$.

next to the subject's unaffected fingers, which connected to the control box via Bluetooth. During the experiment, participants controlled the glove in Button Mode. A 10-minute warm-up session was provided to familiarize participants with the experimental task and practice controlling the glove via the mobile phone. During this phase, participants performed various movements using the gloves, such as making a fist, opening it, holding an apple, and so on. Following this, participants completed two assessment experiments.

Participants completed an assessment experiment to evaluate the motion range of their affected fingers while using the proposed device. The task was performed over three sessions. In the first session, referred to as "Un-Assistive," participants moved their affected finger without wearing gloves. The second session was "Flexion Assisted," in which participants wore a glove on the affected finger and utilized a flexible actuator to assist with the affected finger's movement. The third and final session was "Bidirectional Assist," in which participants wore the glove on the affected finger, and the glove assisted with the affected finger's movement using hybrid actuators.

Each session was divided into two sub-phases:

1) *Rest*: Participants were asked to sit still and relax for 2 minutes.
2) *Task*: Participants completed flexion and extension movements of the affected finger.

Next, participants completed an assessment to measure grip force while using the assisted gloves. This task was performed in two experimental sessions. The first session, "Un-Assisted," involved participants moving their affected finger without wearing gloves. In the second session, "Glove Assisted," participants wore the glove on the affected finger and utilized hybrid actuators to assist with the finger's movement.

Each session was divided into two sub-phases:

1) *Rest*: Participants were asked to sit still and relax for 2 minutes.
2) *Task*: Participants grasped each of the two cylinders and moved their hand upwards until the cylinders were separated from their fingers.

To reduce experimental error, each assessment experiment was repeated three times. Participants were given a five-minute rest period between assessments to ensure consistency in finger movements.

D. Results

1) Scope of Motion Assessment: The experimental results are shown in Table IV. For the index finger without the glove, the average bending ranges of the DIP, PIP, and MCP joints are 11.9 ± 3.9°, 6.8 ± 2.8°, and 11.3 ± 4.6°, respectively. For the thumb without the glove, the average bending angles of the IP, MCP, and CMC joints are 9.6 ± 4.2°, 13.3 ± 3.5°, and 8.5 ± 2.8°, respectively. For the index finger with the flexion actuator, the average bending ranges of the DIP, PIP, and MCP joints are 34.6 ± 4.3°, 41.1 ± 3.9°, and 48.1 ± 3.5°, respectively. For the thumb assisted with the flexion actuator, the average bending angles of the IP, MCP, and CMC are 38.2 ± 5.3°, 14.8 ± 3.5°, and 21.0 ± 4.4°, respectively. Actuators in the flexion direction improve the patient's finger bending angle but do not meet the patient's daily life needs. For the index finger assisted by the bidirectional glove, the average bending angles of the DIP, PIP, and MCP joints are 57.9 ± 7.9°, 68.3 ± 5.3°, and 68.1 ± 5.5°, respectively. For the thumb assisted with the bidirectional glove, the average bending angles of the IP, MCP, and CMC are 64.0 ± 4.4°, 32.6 ± 3.2°, and 38.0 ± 3.9°, respectively. The experimental results show that the patients' finger movement range is greatly improved with the aid of the bidirectional gloves. The bending angles of the glove-assisted fingers are greater than the basic functional motion range of the hand (Index finger DIP: 57°, PIP: 64° and MCP: 40°; Thumb IP: 18°, MCP: 21° and CMC: 5°), which is sufficient to perform more than 90% of ADLs [21], [39].

2) Grip Strength Assessment: The maximum friction that the patient can generate without gloves is 8.4 ± 3.5 N with the 50-mm cylinder and 6.4 ± 1.2 N with the 75-mm cylinder (as shown in Fig. 12). When wearing the gloves, the maximum friction is 21.34 ± 5.8 N with the 50-mm cylinder and 15.6 ± 3.7 N with the 75-mm cylinder. This friction is about same as the maximum friction provided by the actuator. The gloves clearly improve the grip force of the patients' fingers. It is worth noting that the patient wears gloves in the Unassistive situation, which guarantees the consistency of the friction coefficient. The experiment results show that the frictional force provided by the actuator plays an essential role in the patient's grasp. Besides, the friction force generated on the 50-mm cylinder is greater than that generated on the 70-mm cylinder. This conclusion appears to contradict previous research [11]. The underlying reason is that the friction force

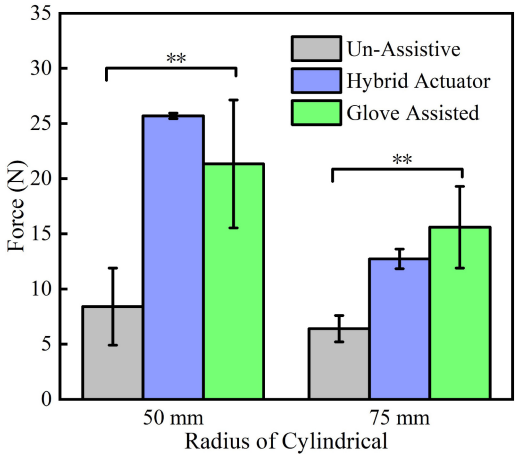

Fig. 12. Friction of the patients' fingers with and without gloves and the actuator. Significant pairs respect to the baseline are presented with different levels: * $p < 0.05$, ** $p < 0.01$.

is related to the contact area, which can be influenced by the length of the actuator or the radius of the grip object.

V. Discussion and Conclusion

This article has described a bidirectional soft glove that assists patients with chronic stroke in their rehabilitation and ADLs. The glove is based on a hybrid actuator that contains flexion and extension actuator units to assist the patient's fingers in two directions. A finite element model was established to optimize the critical parameters, including the radius of the air cavity R_2 and the material of the soft actuator. According to the simulation results, we set $R_2 = 3$ mm and made the actuator out of Dragon Skin 30. This configuration allows the actuator to generate a bending angle of 250° under 150 kPa and achieve a distal side force of 2.8 N. A water-cooling structure was designed to reduce the temperature of the SMA spring actuator, thus increasing the response speed by 55.8%. The obstructed tip force of the actuator reaches 16.02 N at 200 kPa, and the maximum friction force generated by the actuator is 12.72 ± 0.89 N with a 75-mm cylinder and 25.69 ± 0.26 N with a 50-mm cylinder.

Eight stroke patients participated in experiments to verify the performance of the gloves. The results show that the gloves significantly improve the patients' finger motion range and grasping force, and satisfy the needs of rehabilitation and ADLs. An app that can be installed on the patient's mobile phone was also designed to enable better clinical effects, allowing the patient to choose their rehabilitation mode without needing to see a therapist. The control strategies include button mode and mirroring rehabilitation training. These different control strategies help patients with ADLs and rehabilitation training, respectively.

One of the limitations of our study is the size and mass of the proposed hand exoskeleton robot, which currently limits its usability to stationary settings. In the future, we plan to optimize the size and mass of the robot to improve its portability and expand its range of potential applications. Another limitation of our study is the slow response time of the proposed device. The proposed device has a motion cycle of approximately 10 s, which meets the needs of the rehabilitation training. However, this response speed of the robot reduces the speed of the patient's finger movements in the robot-assisted patient's daily life. The slow response speed of the robot limits its use in scenarios that require faster finger movements, such as playing the piano and typing. In the future we will optimize the structure and control algorithms of the hybrid actuator to improve its responsiveness.

To the best of our knowledge, this study represents a pioneering effort in proposing a flexible robot for hand assistance and therapy, utilizing soft materials and memory alloy components. This novel approach in the design and optimization of hybrid actuators, predominantly employing flexible robots and memory alloys, offers several advantages. The hybrid actuator provides a larger working space and output force, thereby enhancing the benefits of robot-assisted hand therapy. The application of this technology extends beyond assistance in daily life activities, as we have also designed a rehabilitation training system incorporating virtual reality, force feedback, and mirror therapy. This integrated approach aims to provide a more comprehensive and effective rehabilitation treatment for patients.

In the future, the control of the actuator needs further research to achieve a more compliant control. As the two actuators drive motion in two directions, the hybrid actuator can work antagonistically to achieve better tracking accuracy and actuator performance.

References

[1] D. Lloyd-Jones et al., "Heart disease and stroke statistics—2010 update: A report from the American heart association," *Circulation*, vol. 121, no. 7, pp. e46–e215, 2010.

[2] G. B. Prange, M. J. Jannink, C. G. Groothuis-Oudshoorn, H. J. Hermens, and M. J. Ijzerman, "Systematic review of the effect of robot-aided therapy on recovery of the hemiparetic arm after stroke," *J. Rehabil. Res. Dev.*, vol. 43, no. 2, pp. 171–84, 2006.

[3] S. Balasubramanian, J. Klein, and E. Burdet, "Robot-assisted rehabilitation of hand function," *Current Opin. Neurol.*, vol. 23, no. 6, pp. 661–70, 2010.

[4] Y.-L. Tsai et al., "Usability assessment of a cable-driven exoskeletal robot for hand rehabilitation," *Front. Neurorobot.*, vol. 13, p. 3, Feb. 2019.

[5] N. Meng, W. Kun, L. Mingxin, Y. Ke, and W. Zhi, "Design, analysis and experiment of finger soft actuator with nested structure for rehabilitation training," *Adv. Mech. Eng.*, vol. 12, no. 11, pp. 1–15, 2020.

[6] C. Correia et al., "Improving grasp function after spinal cord injury with a soft robotic glove," *IEEE Trans. Neural Syst. Rehabil. Eng.*, vol. 28, no. 6, pp. 1407–1415, Jun. 2020.

[7] L. Cappello et al., "Exploiting textile mechanical anisotropy for fabric-based pneumatic actuators," *Soft Robot.*, vol. 5, no. 5, pp. 662–674, 2018.

[8] F. Yang et al., "Design and optimize of a novel segmented soft pneumatic actuator," *IEEE Access*, vol. 8, pp. 122304–122313, 2020.

[9] J. M. Jani, M. Leary, A. Subic, and M. A. Gibson, "A review of shape memory alloy research, applications and opportunities," *Mater. Des.*, vol. 56, pp. 1078–1113, Apr. 2014.

[10] J. F. Farrell, H. B. Hoffman, J. L. Snyder, C. A. Giuliani, and R. W. Bohannon, "Orthotic aided training of the paretic upper limb in chronic stroke: Results of a phase 1 trial," *Neurorehabilitation*, vol. 22, no. 2, pp. 99–103, 2007.

[11] H. K. Yap et al., "A fully fabric-based bidirectional soft robotic glove for assistance and rehabilitation of hand impaired patients," *IEEE Robot. Autom. Lett.*, vol. 2, no. 3, pp. 1383–1390, Jul. 2017.

[12] A. E. Hines, P. E. Crago, and C. Billian, "Hand opening by electrical stimulation in patients with spastic hemiplegia," *IEEE Trans. Neural Syst. Rehabil.*, vol. 3, no. 2, pp. 193–205, Jun. 1995.
[13] C. J. Nycz, T. B. Meier, P. Carvalho, G. Meier, and G. S. Fischer, "Design criteria for hand exoskeletons: Measurement of forces needed to assist finger extension in traumatic brain injury patients," *IEEE Robot. Autom. Lett.*, vol. 3, no. 4, pp. 3285–3292, Oct. 2018.
[14] W. B. Chen, C. H. Xiong, C. L. Liu, P. M. Li, and Y. H. Chen, "Fabrication and dynamic modeling of bidirectional bending soft actuator integrated with optical waveguide curvature sensor," *Soft Robot.*, vol. 6, no. 4, pp. 495–506, 2019.
[15] S. Kazeminasab, A. Hadi, K. Alipour, and M. Elahinia, "Force and motion control of a tendon-driven hand exoskeleton actuated by shape memory alloys," *Ind. Robot*, vol. 45, no. 5, pp. 623–633, 2018.
[16] N. Ma, G. Song, and H. J. Lee, "Position control of shape memory alloy actuators with internal electrical resistance feedback using neural networks," *SmMaS*, vol. 13, no. 4, pp. 777–783, 2004.
[17] B. B. Kang, H. Choi, H. Lee, and K. J. Cho, "Exo-glove poly II: A polymer-based soft wearable robot for the hand with a tendon-driven actuation system," *Soft Robot.*, vol. 6, no. 2, pp. 214–227, 2019.
[18] K. Shi, A. Song, Y. Li, and H. Li, "A cable-driven three-DoF wrist rehabilitation exoskeleton with improved performance," *Front. Neurorobot.*, vol. 15, Apr. 2021, Art. no. 664062.
[19] P. Polygerinos et al., "Modeling of soft fiber-reinforced bending actuators," *IEEE Trans. Robot.*, vol. 31, no. 3, pp. 778–789, Jun. 2015.
[20] L. Saharan, M. J. de Andrade, W. Saleem, R. H. Baughman, and Y. Tadesse, "iGrab: hand orthosis powered by twisted and coiled polymer muscles," *Smart Mater. Struct.*, vol. 26, no. 10, 2017, Art. no. 105048.
[21] G. I. Bain, N. Polites, B. G. Higgs, R. J. Heptinstall, and A. M. McGrath, "The functional range of motion of the finger joints," *J. Hand Surg. Eur. Vol.*, vol. 40, no. 4, pp. 406–11, 2015.
[22] S. Li, D. G. Kamper, and W. Z. Rymer, "Effects of changing wrist positions on finger flexor hypertonia in stroke survivors," *Muscle Nerve*, vol. 33, no. 2, pp. 183–190, 2006.
[23] K. Matheus and A. M. Dollar, "Benchmarking grasping and manipulation: Properties of the objects of daily living," in *Proc. IEEE/RSJ Int. Conf. Intell. Robot. Syst.*, 2010, pp. 5020–5027.
[24] P. Polygerinos, Z. Wang, K. C. Galloway, R. J. Wood, and C. J. Walsh, "Soft robotic glove for combined assistance and at-home rehabilitation," *Robot. Auton. Syst.*, vol. 73, pp. 135–143, Nov. 2015.
[25] B. Mosadegh et al., "Pneumatic networks for soft robotics that actuate rapidly," *Adv. Funct. Mater.*, vol. 24, no. 15, pp. 2163–2170, 2014.
[26] S. Dilibal, H. Sahin, J. O. Danquah, M. O. F. Emon, and J.-W. Choi, "Additively manufactured custom soft gripper with embedded soft force sensors for an industrial robot," *Int. J. Precis. Eng. Manuf.*, vol. 22, no. 4, pp. 709–718, 2021.
[27] D.-S. Copaci, D. Blanco, A. Martin-Clemente, and L. Moreno, "Flexible shape memory alloy actuators for soft robotics: Modelling and control," *Int. J. Adv. Robot. Syst.*, vol. 17, no. 1, p. 19, 2020.
[28] M. Dolce and D. Cardone, "Mechanical behaviour of shape memory alloys for seismic applications 1. martensite and Austenite Ni-Ti bars subjected to torsion," *Int. J. Mech. Sci.*, vol. 43, no. 11, pp. 2631–2656, 2001.
[29] Y. Hao, T. Wang, Z. Ren, M. Planck, and Z. Gong, "Modeling and experiments of a soft robotic gripper in amphibious environments," *Int. J. Adv. Robot. Syst.*, vol. 14, no. 3, 2017, Art. no. 1729881417707148.
[30] Y. Elsayed et al., "Finite element analysis and design optimization of a pneumatically actuating silicone module for robotic surgery applications," *Soft Robot.*, vol. 1, no. 4, pp. 255–262, 2014.
[31] Y.-J. Lai, L.-J. Yeh, and M.-C. Chiu, "An experimental investigation on shape memory alloy dynamic splint for a finger joint application," *Sensors Actuators A Phys.*, vol. 173, no. 1, pp. 210–218, 2012.
[32] Z. Zhang, H. Chen, and Z. Zhang, "Configuration synthesis and performance analysis of finger soft actuator," *Appl. Bionics Biomech.*, vol. 2018, Aug. 2018, Art. no. 4264560.
[33] H. K. Yap et al., "A magnetic resonance compatible soft wearable robotic glove for hand rehabilitation and brain imaging," *IEEE Trans. Neural Syst. Rehabil. Eng.*, vol. 25, no. 6, pp. 782–793, Jun. 2017.
[34] W. D. Fisher and M. S. Mujtaba, "Hybrid position/force control: A correct formulation," *Int. J. Robot. Res.*, vol. 11, no. 4, pp. 299–311, 1992.
[35] J. J. Craig and M. H. Raibert, "A systematic method of hybrid position/force control of a manipulator," in *Proc. IEEE 3rd Int. Appl. Conf. Comput. Softw. Comput. Soc.*, 1979, pp. 446–451.
[36] A. De Luca et al., "Training the unimpaired arm improves the motion of the impaired arm and the sitting balance in chronic stroke survivors," *IEEE Trans. Neural Syst. Rehabil. Eng.*, vol. 25, no. 7, pp. 873–882, Jul. 2017.
[37] C. Dohle, J. Püllen, A. Nakaten, J. Küst, C. Rietz, and H. Karbe, "Mirror therapy promotes recovery from severe hemiparesis: A randomized controlled trial," *Neurorehabil. Neural Repair*, vol. 23, no. 3, pp. 209–217, 2009.
[38] Y. J. Kang et al., "Upper extremity rehabilitation of stroke: Facilitation of corticospinal excitability using virtual mirror paradigm," *J. Neuroeng. Rehabil.*, vol. 9, no. 1, p. 71, 2012.
[39] M. J. Barakat, J. Field, and J. Taylor, "The range of movement of the thumb," *Hand*, vol. 8, no. 2, pp. 179–182, 2013.